Lipids–Fluorophores Interactions Probed by Combined Nonlinear Polarized Microscopy

Paulina Gasecka, Naveen Balla, Miguel Sison, Sophie Brasselet

Lipids-Fluorophores Interactions Probed by Combined Nonlinear Polarized Microscopy

Paulina Gasecka, Naveen K. Balla, Miguel Sison, and Sophie Brasselet*

Aix Marseille Univ, CNRS, Centrale Marseille, Institut Fresnel, F-13013 Marseille, France

E-mail: sophie.brasselet@fresnel.fr

Abstract

Studying the structural dynamics of lipid membranes requires methods that can address both microscopic and macroscopic characteristics. Fluorescence imaging is part of the most used techniques to study membrane properties in various systems from artificial membranes to cells: it benefits from a high sensitivity to local properties such as polarity and molecular orientational order, with a high spatial resolution down to the single molecule level. The influence of embedded fluorescent lipid probes on the lipid membrane molecules is however poorly known and relies most often on molecular dynamics simulations, due to challenges faced by experimental approaches to address the molecular-scale dimension of this question. In this work we develop an optical microscopy imaging method to probe the effect of fluorophores embedded in the membrane as lipid probes, on their lipid environment, with a lateral resolution of a few hundreds of nanometers. We combine polarized-nonlinear microscopy contrasts that can address independently the lipid probe, by polarized two-photon fluorescence, and the membrane lipids, by polarized coherent Raman scattering. Using trimethylamino-derivative 1-(4-trimethyl ammonium-phenyl)-6-phenyl-1,3,5-hexatriene (TMA-DPH) and di-8-butyl-amino-naphthyl-ethylene-pyridinium-propyl-sulfonate (di-8-ANEPPS) as model probes,

we show that both probes tend to induce an orientational disorder of their surrounding lipid CH-bonds in 1,2-dipalmitoylphosphatidylcholine (DPPC) lipids environments, while there is no noticeable effect in more disordered 1,2-dioleoyl-sn-glycero-3-phosphocholine (DOPC) lipid membranes.

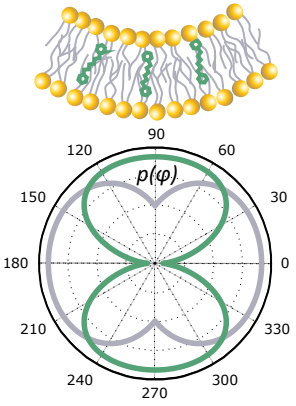

Introduction

In the last decades a multitude of techniques has emerged to study the microscopic behavior of lipids membranes, addressing the spatial and orientational order of lipid molecules as well as their structural and conformational properties. On the atomic scale, nuclear magnetic resonance (NMR)[1,2] and X-ray diffraction[3] are able to deliver quantitative information such as the spatial occupation and organization of lipid molecules, the spacing between lamellas in lipid bilayers stacks and their density profile. Although detailed molecular-scale information on lipids can be obtained, these techniques are often invasive for the sample and cannot be applied to dynamic studies. To provide *in situ* spatio-dynamics observations, optical vibrational spectroscopy methods have been developed based on infrared absorption, Raman scattering or nonlinear sum frequency generation.[4] FLuorescence microscopy is particularly appropriate for the spatio-temporal study of lipid membranes structure and dynamics averaged over spatial scales of a few hundreds of nanometers down to the single molecule level.[5–8] Fluorescence microscopy, which relies on fluorescent reporters to reveal lipid en-

vironment specificies, cover many approaches such as spectrally-resolved polarity-sensitive imaging,[9,10] surface-morphology sensitive total internal reflection fluorescence (TIRF) imaging,[11] diffusion-sensitive fluorescence recovery after photobleaching (FRAP)[12] and fluorescence correlation spectroscopy (FCS),[13] as well as lipid-interaction-sensitive fluorescence resonant energy transfer (FRET).[14]

Among the fluorescence imaging methods dedicated to lipid membrane studies, polarized fluorescence[15,16] is particularly interesting for its ability to quantify the orientational behavior of lipid probes imaged inside a focal spot of typically 300 nm size. The most widely used version of polarized fluorescence imaging in organized structures is linear dichroism, in which a varying incident linear polarization generates a modulation of the fluorescence signal, which amplitude is related to the fluorescent probes' molecular orientational order.[17,18] Recent works also include orientation monitoring of lipid probes at the single molecule level,[5,8] providing a nanometric scale readout of the local membrane structural behavior. Polarization resolved two-photon fluorescence, PR-2PEF, exhibits an additional advantage of being sensitive to higher orders of the molecular angular organization, thanks to the nonlinear optical interaction involved.[19] PR-2PEF has allowed to quantitatively image the local modification of lipid disorder in model giant unilamellar vesicles (GUV), emphasizing different orientation properties in liquid ordered and disordered phases[20] as well as for different membrane voltage-sensitive probes.[21] The approach has been also applied in the plasma membrane of living cells where lipid orientational order is closely related to the cholesterol content,[17] membrane ruffling at the interface between cells[22] or cytoskeleton perturbations.[23]

These techniques, although very powerful, rely on fluorescence dyes inserted into the lipid membrane, which interaction with the surrounding lipids is still poorly known. It is generally assumed that the lipid probe is able, through this interaction, to report on the structural behavior of its surrounding lipids, with concentrations small enough (<2 mol%) to assume that the surrounding lipid environment is actually not affected by the fluorescent probe itself. At

the macroscopic level, studies have reported a very small influence of embedded dyes on the lipids main phase transition temperature,[24,25] a modification of the pressure-area isotherm shape in the liquid-expanded phase[26] or of the bending elasticity of the membrane.[27] At a microscopic scale, early studies have hypothesized possible perturbations induced by probes on lipid membranes, via the influence on their lipid-phase partitioning by their lipid acyl chain nature,[28] the changes in the surface area occupied by lipids in presence of a probe[26] or the lipids orientational order.[29] Recent experimental results on voltage-sensitive lipid probes have also reported a possible influence on their local lipid environment by a visible decrease of the reported local polarity when increasing the dye concentration.[30,31]

Quantifying the extent of the perturbations made by lipid probes on surrounding lipids as well as the scale at which they take place is however still a challenging problem. Quantitative answers to this question have been provided by molecular dynamics (MD) simulations, which bring an atomic-scale level of structural perturbations such as how probes insert and orient in membranes.[32] Studies on the fluorescent probe 1,6-diphenylhexatriene (DPH) have evidenced modifications of the order of neighbour lipids, membrane thickness and area per molecule, which was attributed to the deep insertion of the dye in the membrane.[33] However distant lipids were seen to be unaffected by the presence of DPH, as confirmed by very small changes in DSC and NMR data.[33] Its charged trimethylamino-derivative 1-(4-trimethyl ammonium-phenyl)-6-phenyl-1,3,5-hexatriene (TMA-DPH) is also known to modify DPPC phase transition temperature, which evidences an effect on lipids.[34] MD studies on environmentally sensitive dyes have emphasized the difficulty to tackle the question on both experimental and theoretical sides. MD simulations have shown that the voltage-sensitive probe Prodan increases the degree of hydration of the surrounding lipids upon excitation in lipid bilayers of various compositions, but with a different influence on the lipid orientational order depending on the lipid phases, while experiments show a decrease of polarity in all phases at increasing concentration.[30] Measurements on other voltage-sensitive probes

Laurdan and di-4-ANEPPDHQ also showed discrepancies with simulations,[31] which were attributed to the diversity of locations of lipid probes in the bilayers and by the fact that experiments rely on an indirect probing with probes possibly influencing their own readout by interactions.

In order to evaluate the effect of lipid probes on lipids and vice versa, new approaches are required to measure lipid surroundings organization independently from the signal from lipid probes. To this end, we developed a methodology based on label-free polarization sensitive nonlinear imaging that is compatible with PR-2PEF. This method relies on the detection of chemical vibration bonds via the nonlinear coherent Raman scattering process. Coherent anti-Stokes Raman scattering (CARS) and stimulated Raman scattering (SRS) both take place in a sample illuminated by two focused pulsed synchronized lasers at the Stokes ω_S and pump ω_p frequencies (Fig. 1a). CARS[35,36] results from a nonlinear induced anti-Stokes radiation at the frequency ω_{aS}, which is enhanced at the resonance condition with a molecular vibration frequency Ω_{vib}: $\omega_p - \omega_S = \Omega_{vib}$. In addition to the amplified signal at the vibrational responsance, CARS signals are generally superimposed with the non-resonant electronic response of the system, attributed to a pure four wave mixing signal called non-resonant background. SRS[37,38] is a process similarly occuring from the amplification of the Raman signal, which quantifies the amount of energy transfer from the pump to the Stokes when both beams are in resonance with Ω_{vib}. As a result of this interaction, the pump beam experiences a loss of signal (stimulated Raman loss, SRL), while Stokes beam experiences a gain of signal (stimulated Raman gain, SRG). In SRS, the non-resonant background is significantly reduced compared to that of CARS since the amplification effect does not occur outside of the vibrational resonance. In both processes, the resulting signal is sensitive to the incident (ω_p, ω_S) polarization directions when the probed vibration bonds are oriented, permitting the measurement of the degree of their molecular orientation properties inside a focal spot of typically 300-500 nm lateral size. Provided that molecular bonds are oriented,

such as in lipid layers, this results in a modulation of the detected CARS or SRS intensity, which is maximized when the incident ω_p and/or ω_S polarizations lie along the averaged direction of the bonds' distribution. Using polarization-resolved CARS (PR-CARS), the molecular orientational order of CH2 vibrational stretching bonds in lipids has been quantified in artificial bilayers[39–41] and multilayers,[42–45] where it was found that the lipid phase environment as well as the presence of cholesterol strongly influences the width and shape of the bonds angular distribution. Lipid orientational order imaging by PR-CARS has also been applied in myelin, which forms dense lipid multilayers around axons in brain and spinal cord tissues.[46–50] In contrast to PR-CARS, PR-SRS has been more rarely investigated.[51–53] It has been shown however that this process in membranes, being less sensitive to background from non-resonant electronic four wave mixing processes, is a more reliable quantification of lipid orientational order.[45]

In this work, we focus on multilamellar vesicles (MLVs) as a model system to address the question of the influence of lipid-probes on the organization of lipids in artificial membranes (Fig. 1b). MLVs are made of multiple lipid bilayers with the aqueous solution trapped in between. MLVs are micrometric size, accumulating bilayers of about $4-5$ nm thinckness, with a spacing between layers of about 1.5 to 3 nm.[3] Even though CARS has been demonstrated down to the scale of lipid bilayers,[40,41,54] MLVs are more adapted to sensitive PR-CARS/SRS microscopy than unilamellar vesicles due to the larger number of CH bonds in the focal volume in multilayers, they are also convenient to immobilize in a non-invasive way. It has been shown[3] that interactions between bilayers in fully hydrated MLVs have negligible effect on the intrinsic structure of the bilayers, which might be the first concern when dealing with MLVs. MLVs of different lipid phase natures are investigated in this work at room temperature, from disordered pure fluid liquid-disordered L_d phases in dioleoylphosphatidylcholine (DOPC), to gel solid-ordered S_o phase in 1,2-dipalmitoyl phosphatidylcholine (DPPC). These phase behaviors are characteristic of different lateral and orientational orga-

nizations of lipids, which occupy larger areas and undergo larger orientational fluctuations in liquid disordered environments depending on the degree of saturation of their acyl chain and their length.

Fluorophores were selected for their high quantum yield and large nonlinear absorption cross section making these molecules suitable for two-photon excitation, their parallel orientation to the axis of the hydrocarbon chains of lipids inside the membrane, and their partitioning in both L_d and S_o phases. We concentrated on two widely studied membrane probes. TMA-DPH, which is a derivative of DPH that has been partially documented with respect to its possible influence on its lipids surrounding, and di-8-butyl-amino-naphthyl-ethylene-pyridinium-propyl-sulfonate (di-8-ANEPPS), a well reported voltage-sensitive probe exhibiting a spectral sensitivity to local polarity.[55] In TMA-DPH a cationic group is purposely placed to anchor the DPH probe close to the water/bilayer interface, in contrast with pure DPH which locates deeper in the hydrophobic core of the bilayer. TMA-DPH is present in all lipid phases with an orientational constraint highly sensitive to the lipid phase due to strong electrostatic interactions with lipids,[25,56–58] making it an interesting reporter of membrane fluidity.

In this work, we apply the combination of PR-2PEF and PR-CARS/SRS to the investigation of the mutual influence of the TMA-DPH and di-8-ANEPPS probes with lipids, probing the dyes orientational distributions by PR-2PEF and the surrounding CH vibrational bond distributions by PR-CARS/SRS. We confirm that PR-SRS is a more appropriate contrast to study unbiased lipid orientational order in MLVs, and use this contrast to investigate the influence of the presence of the lipid probes on the intrinsic lipid organization. We investigate the influence of TMA-DPH and di-8-ANEPPS on disordered and ordered lipid phases present in DOPC and DPPC. We show that the orientational order of dyes probed by PR-2PEF is generally more heterogeneous than the pure lipid orientational order probed by PR-SRS, and that both respond to lipid phase changes in a very close proportion. When

comparing labelled and unlabelled MLVs, we show that the pure lipid orientational order is not significantly influenced by the presence of the dye in disordered lipid phases of DOPC MLVs, however it shows a higher degree of orientational order in ordered lipids in DPPC MLVs. This study shows the ability of this approach to investigate, at large scales and with spatial resolution of a few hundreds of nanometers, the influence of fluorescent probes on the lipids structural behaviors in membranes.

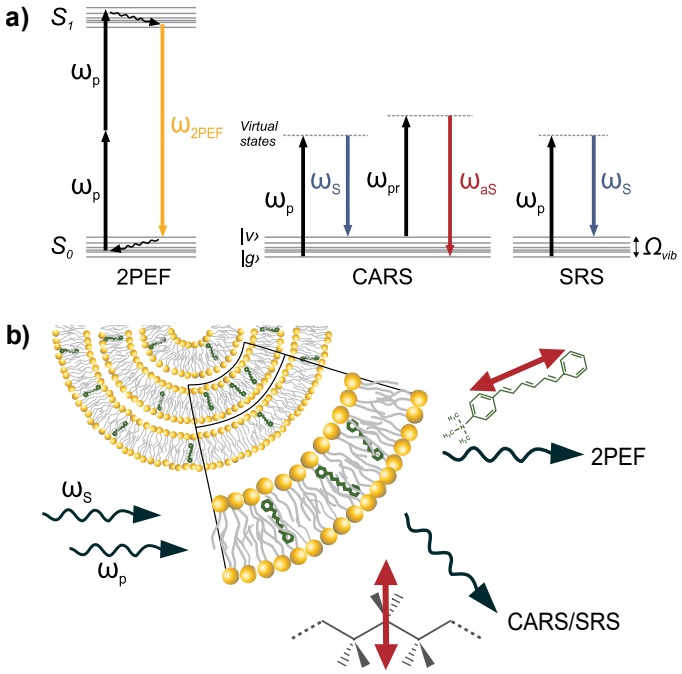

Figure 1: (a) Enegry level diagrams represented for the different nonlinear optical processes used in this work: 2PEF, CARS and SRS, involving the pump and Stokes frequencies ($\omega_p = \omega_{pr}, \omega_S$) which difference falls in responance with the vibrational frequency Ω_{vib}. (b) Schematic structure of the investigated MLVs, with the molecular structures TMA-DPH and CH bonds responding to the different optical signals investigated. The red arrows corresponds to the orientation monitored by the polarization resolved contrast: absorption transition dipole for PR-2PEF, CH vibration bonds direction for PR-CARS/SRS.

Methods

MLV samples preparation

In order to investigate molecular order of lipids in labelled and unlabelled membranes, we choose structurally similar phospholipids exhibiting different phases at room temperature (T=21 ± 1°C): 1,2-dipalmitoyl phosphatidylcholine (DPPC) and dioleoylphosphatidylcholine (DOPC). All phospholipids were purchased from Avanti Polar Lipids, stored in −20°C and used without further purification. 1-(4-trimethyl ammonium-phenyl)-6-phenyl-1,3,5-hexatriene (TMA-DPH), was purchased from Sigma Aldrich and di-8-butyl-amino-naphthyl-ethylene-pyridinium-propyl-sulfonate (di-8-ANEPPS) from Fisher Scientific. Multilamellar vesicles (MLVs) were prepared according to the hydration method developed by.[59] First, 100 μl of 10 mM solution of phospholipid, pure or mixed with 1 mM solution of the fluorescent probe were used to obtain the molecular ratio of 1 : 1000 to 10 : 1000. The solution was immediately evaporated under a nitrogen stream and then vacuumed for 3 h. The dried phospholipid-fluorophore films were then hydrated (1 h) either in phosphate-buffered saline (PBS, pH 7.4) or in a pure water (miliQ) or in the case of DOPC lipids in 1% agarose in pure water (miliQ) above the main phase transition temperature, gently shaking from time to time. The resulting MLVs were of different size ranging between 1 and 30 μm. For the experiments, a small amount of a suspension was placed between two coverslips separated by 100 μm spacers. In the case of DOPC this suspension was gently heated above the gelling temperature of agarose (T=25 ± 5°C) in order to fix MLVs, preventing their motion. We ensured that all PR measurements data given by MLVs immobilized in agarose were identical to those deposited in PBS or water. All data were measured on MLVs of 5 to 15μm size, at room temperature (T=21 ± 1°C).

Experimental setup

The light source is a tunable mode-locked Ti:Sapphire laser (Chameleon Ultra II, Coherent Inc.) operating in the range from 690 to 1080 nm which delivers 150 fs pulses (repetition rate 80 MHz) to an optical parametric oscillator (Compact OPO-Vis, Coherent Inc.) with an output average power of 5 W. The pump (ω_p) and the Stokes (ω_S) beams can be individually tuned and are extracted from the Ti:Saph and the OPO output beams, respectively. The beams wavelengths are chosen to target the CH bonds stretching vibration frequency (centered at 2845 cm^{-1}). In the used fs regime, this excitation wavelength range covers CH_2 symmetric and antisymmetric stretching vibrations as well as CH_3 vibrations for CARS and SRS measurements, together with the excitation of the TMA-DPH dye (2PEF excitation: $\approx$ 780 nm, fluorescence emission $\approx$ 450 nm) and di-8-ANEPPS (2PEF excitation $\approx 780 - 900$ nm, emission $\approx$ 630 nm) for 2PEF measurements. A pump wavelength of 780 nm was therefore used together with a Stokes wavelength of 1002 nm, which gives rise to a CARS emission wavelength of 639 nm. This wavelength is spectrally distinct from the TMA-DPH fluorescence emission so that no spectral overlap is expected between these signals. For experiments involving di-8-ANEPPS, due to spectral overlaps of CARS and 2PEF signals, only SRS was considered to probe the lipids orientational order. Both beams, the pump and the Stokes are overlapped in time and space on a reflective protected silver mirror and sent to an inverted microscope (Eclipse Ti, Nikon Instruments Inc.) using a pair of galvonometric scan mirrors (6215H, Cambridge Technology Inc.). The excitation light is focused on the sample by a high numerical aperture objective (NA 0.75, 20x, Nikon Instruments Inc.) and the emitted light is collected in the forward direction by a high numerical aperture objective (NA 1.0, 60x, Nikon Instruments Inc.). The nonlinear signal is recorded with photomultiplier tubes (PMTs, Hamamatsu R9110) to collect the fluorescence (ω_{2PEF}) or the anti-Stokes (ω_{as}) signal in the CARS operation mode while photodiodes (DET100A, Thorlabs) and a fast lock-in amplifier (APE) are used collect the SRS signal. The signals are split using optics of adequate characteristics (605LP dichroic mirror for the CARS/2PEF separation for

TMA-DPH, removable protected silver mirror for CARS/SRS separation). Band-pass filters are used for detected signals to avoid cross talks between their spectral channels: short-pass filters (700SP, Thorlabs) for CARS/2PEF, with additional BP629/53 (Semrock) for CARS, 850LP (Thorlabs) for SRS, FBG37 (Thorlabs) for 2PEF TMA-DPH and BP609/180 (Semrock) for 2PEF di-8-ANEPPS, covering the whole spectrum independently on its lipid phase location. Scanning and data acquisition is performed using an in-house LabVIEW (National Instruments Corp.) program .[60] The image acquisition was performed with a pixel dwell time from 20 to 50μs, over 100 $\times$ 100 pixels, corresponding to a scan ranges of 10 to 50 μm and typical powers at the focal spot of 2 to 10 mW. For SRS, the pump beam is tuned in frequency and modulated in amplitude by an acousto-optic modulator (AOM AAOpto-electronic MT200, 20 MHz). The spatial resolution in 2PEF is estimated to sizes of about 440 nm lateral and 1.7 μm axial for 2PEF, by imaging 100 nm size fluorescent beads. The CARS/SRS resolution is expected to be very close to these values.The measurement time for a polarization resolved image is typically 10 seconds.

To perform the PR measurements, a polarizing beamsplitter (PBS252, Thorlabs Inc.) after the scanning mirrors ensures that the input polarization is properly linearly polarized when reflected on the incident reflection mirror along its p or s polarization direction. An achromatic half-wave plate HWP (AQWP10M-980, Thorlabs Inc.) is placed after this mirror, mounted on a motorized rotational mount (PR50CC, Newport Corp.) to rotate simultaneously both linearly pump and Stokes beams (Fig. 2a). By changing the polarization angle α of the incident pump and Stokes electric fields (E_p and E_S) with respect to the X axis (horizontal axis in the sample image) we record the image for each polarization state over the range of 0° to 170° with an α angle step of 10°. We firstly recorded the polarisation-resolved 2PEF signal using only the (ωp) exciting beam, the second beam (ωS) was then added to for CARS and SRS measurements. Simultaneous measurements could also be performed with similar results. The number of incident α angles of the rotating polarized fields (typically 18) and the incident power are chosen so that the signal does not bleach during the measurement,

providing a signal to noise above 5 to ensure sufficient precision on the retrieved parameters. The rotating HWP is placed just before the focusing objective, resulting in linear excitation polarization free of distortions. The emitted nonlinear signal is detected in forward configuration without any analyzer in the detection path. It has been shown in particular that un-analyzed detection permits to avoid artifact effects from scattering.[61] Note that the forward configuration was favored in the present work, however similarly the epi-detection configuration of a microscope can be used, providing that the adequate reflective optics is used to reflect the incident beams and collect the required wavelengths.

Data processing and analysis

The quantification of the molecular orientational order measured from PR-CARS, PR-SRS and PR-2PEF in MLVs follows the principle derived in[45] and[19] (see details in the Supporting Information). Briefly, each pixel of an image is a recorded PR stack of images, from which we retrieve the modulation of the signal as a function of the input polarizations angle α. First, we ensured that the image stack measured from a PR measurement has not drifted laterally. A slight drift, happening rarely, can nevertheless be corrected for by images registration as a pre-processing step. To retrieve the molecular organization parameters from the PR measurements, we model the optical processes as a dependence to an incoming rotating linear polarizations $E_p(\alpha)$ and $E_S(\alpha)$. In all optical contrasts considered in this work, the intensity signal $I(\alpha)$ contains powers of cosine and sine functions (see Supporting Information), they can therefore be decomposed in a Fourier series as follow:[19,45]

$$I(\alpha) \propto 1 + \sum_{n=1}^{+\infty} [a_n \cos(n\alpha) + b_n \sin(n\alpha)] \tag{1}$$

where $n = 2, 4$ for PR-SRS and PR-2PEF, and $n = 2, 4, 6$ for PR-CARS (see Supporting Information). The Fourier coefficients (a_n, b_n) are estimated by $a_n = \frac{2}{I_0} \sum_{i=1}^{N} I(\alpha_i) \cos(n\alpha_i)$ and $b_n = \frac{2}{I_0} \sum_{i=1}^{N} I(\alpha_i) \sin(n\alpha_i)$ with the total intensity $I_0 = \sum_{i=1}^{N} I(\alpha_i)$. The retrieved co-

efficients (a_n, b_n) are then interpreted as characteristics of the angular distribution function of dipoles constituting the molecular system (red arrows in Fig. 1b), either the absorption transition dipole of fluorophores (PR-2PEF) or the nonlinear induced dipole from CH vibrations bonds of the surrounding lipids (PR-CARS, PR-SRS). This distribution function can be written as a decomposition over symmetry orders of a reduced 2D in-plane distribution $\widetilde{p}(\varphi)$ with φ the orientation of the molecular dipoles in the sample plane (see Supporting Information):

$$\widetilde{p}(\varphi) = p_0 + p_2\cos(2\varphi) + q_2\sin(2\varphi) + p_4\cos(4\varphi) + q_4\sin(4\varphi) \tag{2}$$

p_0 quantifies the amount of isotropy in the distribution, (p_2, q_2) its amount of anisotropy, and (p_4, q_4) the increased order of complexity of the function. The amplitudes of second and fourth order symmetry contributions can be quantified by symmetry molecular orders S_2 and S_4 of orientation φ_2 and φ_4:

$$S_2 = \frac{1}{p_0}\sqrt{(p_2^2 + q_2^2)};\ S_4 = \frac{1}{p_0}\sqrt{p_4^2 + q_4^2}. \tag{3}$$

and

$$\varphi_2 = \begin{cases} \frac{1}{2}\arctan(q_2/p_2), & \text{if } p_2 > 0 \\ \frac{1}{2}\arctan(q_2/p_2) + \frac{\pi}{2}, & \text{else} \end{cases} \tag{4}$$

$$\varphi_4 = \begin{cases} \frac{1}{4}\arctan(q_4/p_4), & \text{if } p_4 > 0 \\ \frac{1}{4}\arctan(q_4/p_4) + \frac{\pi}{4}, & \text{else} \end{cases}. \tag{5}$$

Note that by definition of a positive measured intensity, the range of values for S_2 and S_4 is confined within [0-2].

These four independent parameters play distinct roles in the description of the distribution function. The angle φ_2 reports the main orientation of the distribution and S_2 reports

the degree of anisotropy of the distribution regardless its orientation. S_4 is attributed to higher angular frequencies and thus to more complex details in the shape of the distribution. A smooth Gaussian-like distribution will for instance contain less fourth order symmetry than a distribution with sharper edges such as a cone. The order 4 orientation φ_4 plays also a role in the shape distribution: if φ_4 is along φ_2, the distribution is of cylindrical symmetry. If not, the distribution becomes asymetric. It is thus convenient to separate this degree of symmetry into two new coefficients for S_4, one symmetric ($S_4^{(s)}$) and one antisymmetric ($S_4^{(a)}$):[19]

$$S_4^{(s)} = S_4 \cos(4(\varphi_4 - \varphi_2)); \; S_4^{(a)} = S_4 \sin(4(\varphi_4 - \varphi_2)). \tag{6}$$

$S_4^{(a)}$ is non-vanishing only for asymmetric distributions.

The parameters S_2 and S_4 holds therefore not only information on the disorder of the angular distribution (its angular aperture), but also on its shape, making more obvious the apparition of sharper features and of asymmetry. In order to provide a concrete readout of this distribution from its symmetry orders, we introduce a super-Gaussian function centered on φ_0 and of width σ; with a steepness a characteristic of the sharpness of the angular constraint undergone by the dipoles present in this distribution:

$$\widetilde{p} \propto e^{-(|\varphi-\varphi_0|/2\sigma)^a} \tag{7}$$

where the $\propto$ sign contains a normalization factor. The width of the distribution decreases with σ, and its shape gets sharper with a, from a Gaussian (a=2) to a sharp cone (a=100). A contribution from an isotropic distribution of dipoles can be added to this function, in order to represent possible overlapping populations on the top of ordered population (see Supporting Information). This can be the case when lipid layers are locally disorganized such as observed in myelin in tissues,[49] or when fluorescent molecules internalize in the membrane.

The determination of the orientational order parameters (S_n, φ_n) from the measured (a_n, b_n) coefficients is dependent on the optical contrast considered. A simple theoretical

framework has been developed to relate these quantities from linear expressions in CARS, SRS and 2PEF signal (see Supporting Information).

At last we estimated the precision and accuracy of the measurement using a model sample made of a drop of olive oil placed on the coverslip. This sample was chosen for its high CARS/SRS sensitivity in the CH stretching vibrations region at 2845 cm^{-1}, and its isotropy which produces S_2 and S_4 magnitudes dependent only on the intensity level not the directionality of the sample itself. The S_2 and S_4 parameters, expected to be 0, as well as their standard deviations, decrease when the level of the intensity increases. The values are ranging from 0.12 ± 0.06 (lowest intensity) to 0.02 ± 0.01 (highest intensity) for S_2 and 0.47 ± 0.26 to 0.08 ± 0.04 for S_4, respectively. In the present work, we tuned the experimental conditions to reach signal levels that lead to an estimation of orientational order parameters with a variance no more than 0.02 for S_2 and 0.07 for S_4, and a bias lower than 0.05 and 0.1 for S_2 and S_4 respectively.

Results and discussion

Combined nonlinear PR-CARS, PR-SRS and PR-2PEF signals provide complementary molecular orientational order information.

TMA-DPH labelled MLVs were investigated combining three nonlinear PR contrasts, PR-CARS, PR-SRS and PR-2PEF, to investigate the molecular orientational order of both lipids and fluorophores and their mutual orientational effect inside multilayered model membranes. The difficulty of such a multimodal experiment comes from the fact that all three collected signals need to be set at optimal spectral regimes such that a) the combination of wavelengths excites both lipids and fluorophores ($2\omega_p$ for 2PEF, ω_p and ω_S for CARS-SRS), b) emission spectra are spectrally well separated, and c) emitted signals are in the range of the maximal efficiency of collecting detectors, in particular for CARS and SRS. All three conditions were fulfilled when performing experiments on MLVs labelled with TMA-DPH,

addressing simultaneously coherent Raman from CH bonds. We could observe that for dyes which wavelength range is closer to the CARS emission, a pre-bleaching of the molecules can be performed nevertheless for the study of labelled MLVs in order to remove the spectral fluorescence contribution in the CARS channel. This procedure, tested for TMA-DPH, was seen to not affect the lipid orientational order as measured by SRS.

Fig. 2b shows the typical level of signal recorded in PR-CARS, PR-SRS and PR-2PEF recorded on a TMA-DPH labelled DPPC-MLV. The signals from the equatorial plane of the MLV for all nonlinear processes is well above the background with an approximate signal to noise ratio of 15. We ascertain that the two-photon absorption process does not affect the SRS data:[62] indeed results are the same before and after bleaching the fluorescence dye. PR-responses polar plots (Fig. 2b) obtained at a given pixel location at the equatorial plane of the MLV exhibit a high modulation for all contrasts. The MLV presented in Fig. 2 shows a very bright border, while other MLVs depicted a more filled composition with a high signal in the interior of the structure as well. In both cases, the inner-peripheral part of the MLV was used for the quantification of molecular order, with similar results for filled and not-filled MLVs. The surrounding background, observable in CARS due to non-resonant contributions, shows no polarization dependence, as expected from an isotropic medium. Fig. 2c depicts combined molecular orientational order and orientation information represented by sticks which orientation in the image plane is the measured φ_2 value at a given pixel location, and which color is the measured S_2 value. The parameters (S_2,φ_2) are depicted only at pixels which total intensity (summed over all (α) incoming angles) is above a given threshold, set to 75% of the maximum total intensity, to emphasize the membrane PR response.

Fig. 2c,d shows that the PR-CARS response is the signature of highly oriented nonlinear CH-bond dipoles along the membrane contour, consistent with previous studies.[39,40,43,44,63] The PR-SRS response depicts a even higher modulated contrast with a higher S_2 value (Fig. 2e,f). This is explained by the presence of a non-resonant contribution in the CARS response coming from the electronic FWM response of the lipids.[45] This non-specific elec-

tronic response is likely to be poorly ordered similarly to what was observed in,[44] which explains the lower orientational order visible in the CARS contrast. As a result, PR-SRS is more appropriate to quantify lipids molecular orientational order via their CH-bonds orientations. In contrast with PR-CARS/SRS responses, the PR-2PEF modulation is oriented with a φ_2 angle perpendicular to the membrane contour (Fig. 2g,h), consistent with the fact that the TMA-DPH the fluorescent dipoles are aligned along the lipid acyl chain direction.[20,56]

PR-SRS in unlabelled MLVs reveals CH-bonds orientational order sensitivity to lipid phases.

Polarization-resolved CARS in lipid layers is known to be dependent on the lipids phase behavior,[39,40,43,44,49,63] however the presence of a non-resonant background in CARS only allows relative qualitative information. The quantification of lipid orientational order using PR-SRS in different lipid environment is less known. We therefore first compared PR-CARS/SRS measurements on different unlabelled MLVs species, made of pure DOPC and DPPC lipids.

Regions of interests were selected around the MLV contours (insets in Fig. 2c,e,g), from which each pixel revealed a set of parameters (S_2, $S_4^{(s)}$, $S_4^{(a)}$). From these pixels collections, 2D graph of $S_4^{(s)}$ as functions of S_2 are represented in Fig. 3, with the goal to quantify which orientational distribution CH-bonds experience on average. As expected, S_2 values from PR-CARS (Fig. 3a) are always slightly lower than from SRS (Fig. 3c) (with a high statistical significance) due to the non-resonant background present in the sample, contrary to SRS response which is a background free. Nevertheless, both CARS and SRS signals follow the same trends when lipids change, which confirms that CARS can be valid for relative measurements.

The distribution of observed data points also exhibits a high level of heterogeneity in the MLVs, which standard deviation surpasses the width expected from noise. This is not surprising considering the complex morphology of multilayers of lipids. On average however,

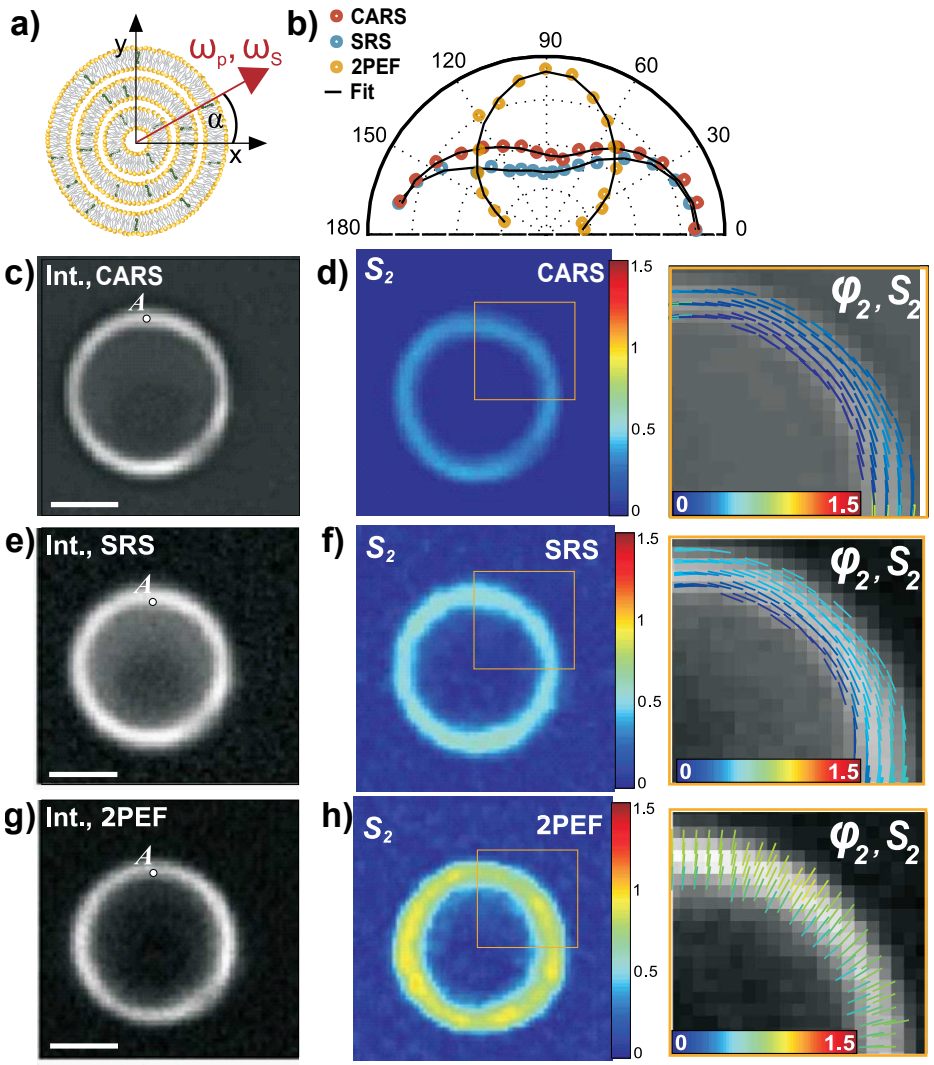

Figure 2: Comparison of typical PR- CARS, SRS and 2PEF results preformed on a single TMA-DPH-labelled MLV made of DPPC lipids. (a) Schematic illustration of PR-measurement in 2D plane of the equatorial plane of an MLV; (ωp, ωS) represent excitation fields and α the incident polarization angle. (b) Polar plots showing the polarization - dependent intensity modulations taken at the point A on the intensity images of the MLV (CARS in (c), SRS in (e), 2PEF in (g)). (c, d) PR-CARS intensity image, summed over all polarization angles α, and the deduced S_2 image. (e, f) Equivalent PR-SRS intensity image and the deduced S_2 image. (g, h) Equivalent PR-2PEF intensity image and the deduced S_2 image. Right: zooms on squares depicting the
φ_2 representation of average orientation of molecular dipoles (illustrated by sticks on pixels which intensity is higher than 75% of the maximum total intensity), CH vibrational bonds for PR- CARS and SRS and TMA-DPH for 2PEF, whose colors follow the S_2 colorscale. Scale bar: 3µm.

the CH molecular bonds orientational order deduced from PR-SRS display in all systems a relatively large level of anisotropy, manifested by S_2 values above 0.2. The $S_4^{(s)}$ and $S_4^{(a)}$ values are in comparison very low (< 0.08), signature of a smooth angular distribution (see Supporting Information). At last, $S_4^{(a)}$ values are centered on zero (see Supporting Fig. S3), similarly as was observed in.[45] This is a signature of angular distribution of cylindrical symmetry, expected from the arrangement of the CH molecular bonds in the MLV geometry.

The S_2 and S_4 values can be directly related to angular distribution functions of known shapes (sharpness a) and disorder (width σ) with a potential isotropic contribution (see Eq. 7 and Supporting Information). Fig. 3 depicts several ($S_4^{(s)}$,S_2) dependencies expected from standard distribution functions. All measured cases are close to Gaussian distributions, superimposed to a isotropic distribution to fit the low S_4 values measured (generally up to a portion of 35% is taken by this isotropic contribution). This contribution is most probably due to morphological properties of MLVs, which include lipid membrane folds that are conserved whatever the lipid phase that is related to the multilamellar nature of the sample. MLVs made of DOPC, which are supposed to be the most disorganized due to the single double-bound in the acyl chain, display the highest orientational disorder ($\sigma \approx 80°$ from PR-SRS) compared to DPPC ($\sigma \approx 66°$ from PR-SRS). This value in DPPC is closed to what has been reported.[45] DPPC made MLVs exhibit a higher orientational order which is attributed to the more rigid structure of this lipids. The distributions expected from the measured molecular orientational order values are represented in Fig. 3b,d, with parameters summarized in Supporting Table S1.

PR-2PEF in labelled MLVs reveals sensitivity of TMA-DPH orientational order to lipid phases.

We then investigated the molecular order reported by the TMA-DPH lipid probes in similar MLVs. Similarly as above, we investigated regions of interest over labelled DPPC and DOPC MLVs, comparing (S_2, $S_4^{(s)}$) amplitudes from PR-2PEF contrasts. PR-2PEF analysis reveals

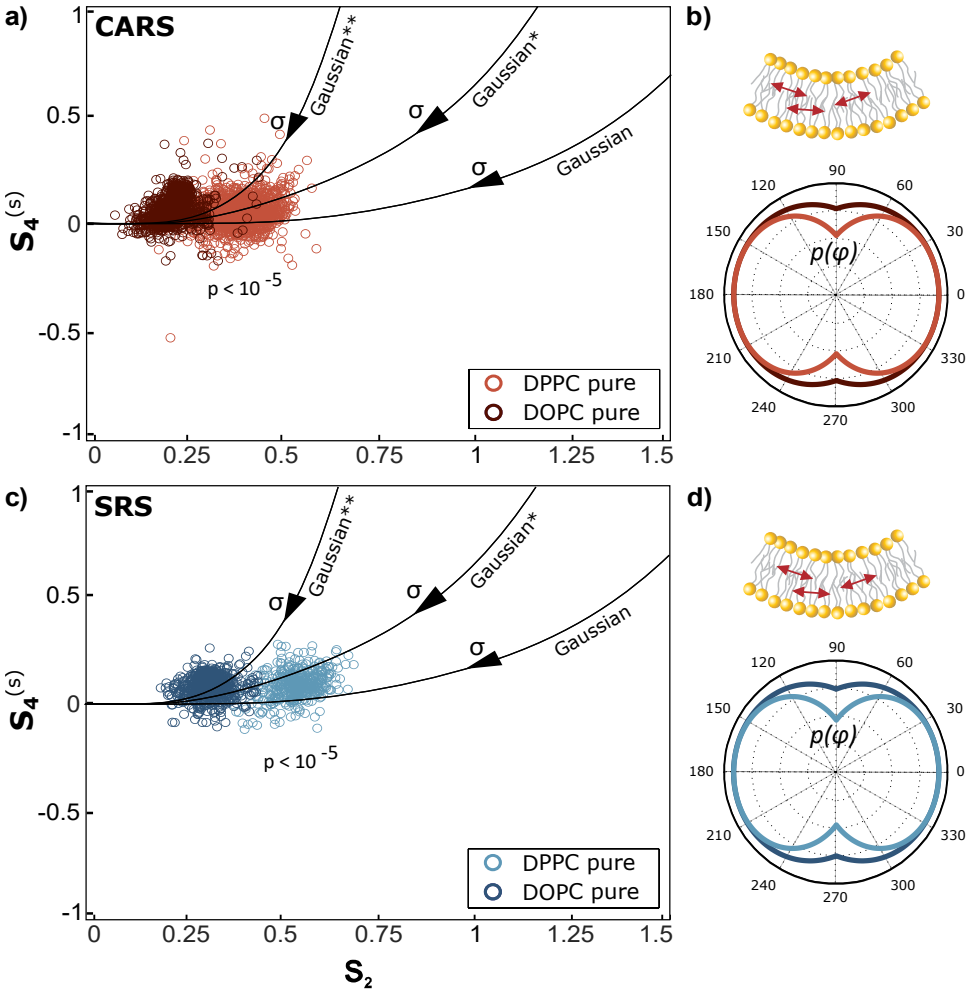

Figure 3: (a) Experimental values of S_2 versus $S_4^{(s)}$ for unlabelled MLVs made of DOPC and DPPC lipids probed by PR-CARS and PR-SRS. Solid lines: theoretical (S_2, $S_4^{(s)}$) for a Gaussian function with 0%, 25% ($*$) or 50% ($**$) contribution from an isotropic population. (b) Corresponding plot of distribution function $p(\varphi)$ of CH molecular bonds (marked as double arrow above the plot) of DOPC (dark red, $\sigma = 86°$, Gaussian with 35% of isotropic population) and DPPC (light red, $\sigma = 73°$, Gaussian with 12% of isotropic population) lipids. (c, d) Identical analysis for PR-SRS for MLVs made of DOPC (dark blue, $\sigma = 80°$, Gaussian with 35% of isotropic population) and DPPC (light blue, $\sigma = 66°$, Gaussian with 12% of isotropic population) lipids. About 15 MLVs per type were measured, using 800 to 1000 pixels per MLV. Statistical significance was determined using ANOVA tests performed over those populations with $p < 0.05$ considered as statistically significant; $p < 0.01$ as highly statistically significant; $p < 0.001$ as extremely statistically significant.

$S_4^{a)}$ values very close to 0, signature of a symmetric distribution along the membrane normal-direction. The resulting distribution of (S_2, $S_4^{(s)}$) order parameters display, on average, a higher orientational order than the CH-bonds measured by PR-SRS, together with a much larger heterogeneity (Fig. 4a,c). In addition, the retrieved $S_4^{(s)}$ values reach non-negligible negative values that cannot be attributed to a smooth Gaussian function as for the CH-bonds distribution. The reported distribution rather fits with a function resembling a smooth cone (in between a Gaussian and a cone distribution) with a non-negligible steepness ($a = 3$) in DPPC, with an average width of $\sigma \approx 48°$(represented in Fig. 4b). This striking difference with the CH-bonds molecular order displayed in Fig. 4d is the signature of different structural properties. TMA-DPH, embedded in lipid membranes features a much lower angular freedom imposed by the surrounding lipids and their interactions with them. The CH molecular bonds of acyl chains in contrast, undergo a higher angular freedom reflected by possible conformational changes as well as the local lipids interactions. The molecular orientational order undergone by TMA-DPH is seen to be quite different in MLVs made of DOPC lipids (Fig. 4a), where the distribution is smoother (closer to a Gaussian function), and more open with $\sigma \approx 65°$(Fig. 4b). This is expected from the surrounding fluid liquid phase and the known sensitivity of TMA-DPH to its lipid environment .[25]

The measured parameters in labelled MLVs are summarized in Supporting Table S1. The results show that 1) TMA-DPH fluorophores are more ordered than their surrounding CH-bonds in lipids, 2) PR-2PEF and PR-SRS are quite equivalent in terms of shifts of order induced by a change of lipid phase (an increase of S_2 from DOPC to DPPC is seen with a factor of 1.6 and 1.8 for TMA-DPH and CH-bonds respectively), 3) the TMA-DPH order is moreover clearly more heterogeneous than that of CH-bonds, which shows that it is not necessarily the most reliable signature of the statistical behavior of lipid molecular order in MLV lipid systems, most probably due to possible internalization of the dye.

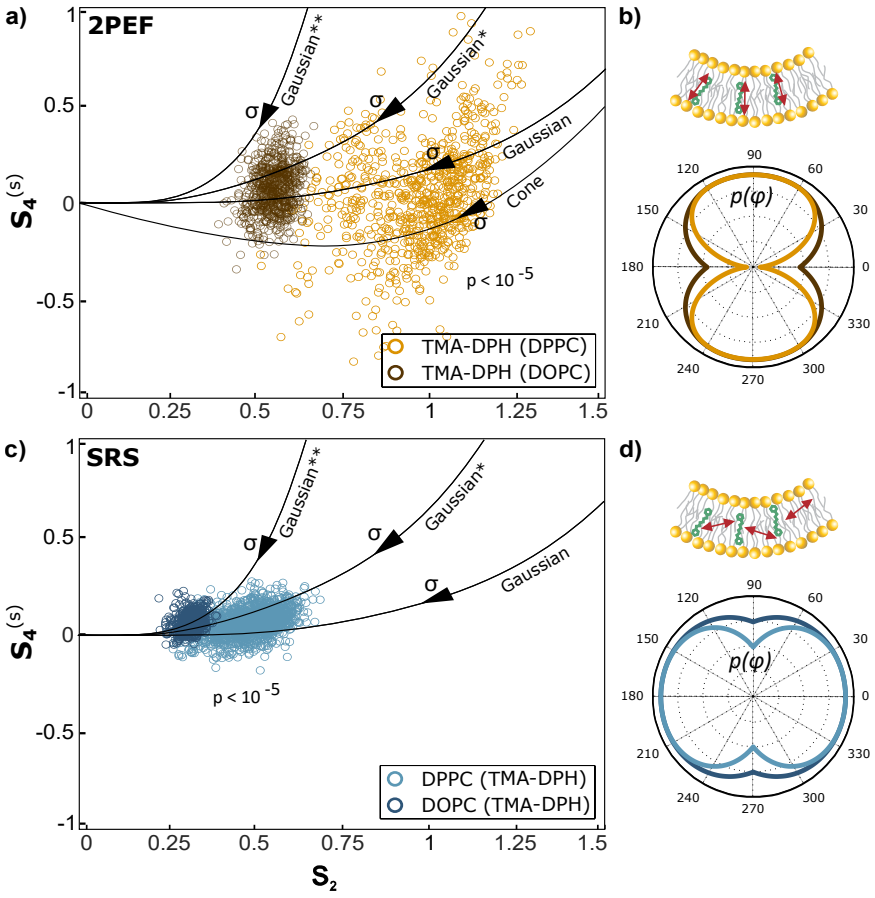

Figure 4: (a) Experimental values of S_2 versus $S_4^{(s)}$ for MLVs made of DOPC and DPPC lipids labelled with TMA-DPH probed by PR-2PEF and PR-SRS. Solid lines: theoretical (S_2, $S_4^{(s)}$) for a Gaussian function with 0%, 25% ($*$) or 50% ($**$) contribution from an isotropic population and a cone (super-Gaussian) with a steepness $a = 3$. (b) Corresponding plot of distribution function $p(\varphi)$ of TMA-DPH fluorophore (dipole marked as double arrow above the plot) embedded in MLVs made of DOPC (dark yellow, $\sigma = 65°$, Gaussian with 12% of isotropic population) and DPPC (light yellow, $\sigma = 48°$, super-Gaussian with steepness $a = 2.5$ and 0% of isotropic population) lipids. (c, d) Identical analysis for PR-SRS probing CH molecular bonds in labelled MLVs made of DOPC (dark blue, $\sigma = 80°$, Gaussian with 35% of isotropic population) and DPPC (light blue, $\sigma = 69°$, Gaussian with 12% of isotropic population) lipids. About 15 MLVs per type were measured, using 800 to 1000 pixels per MLV. Statistical significance was determined using ANOVA tests performed over those populations with $p < 0.001$ considered as extremely statistically significant.

PR-SRS and PR-2PEF reveal sensitivity of CH-bonds order to fluorescence labelling.

These results show that while fluorescent lipid probes reveals a certain molecular organization that can be attributed to its lipid environment, the value of its own orientational order is not quantitatively related to the value of the orientational order of the surrounding lipids. While the influence of the surrounding lipids is known to affect the orientational order of lipid probes, it is equally important to address if the presence of the lipid probe affects the molecular orientational order of the surrounding lipids they are supposed to report on. The method proposed in this work provides the possibility to address this question, since lipids organization can be monitored from a label-free PR-SRS approach in parallel to PR-2PEF experiments. Note that the lipid probes concentration at which the experiments are performed are typical to imaging experiments, considered as sufficiently low to not induce a strong interaction effect between molecules.

We monitored the combined molecular orientational order of CH-bonds in lipids and fluorophores TMA-DH and di-8-ANEPPS probes in the same labelled MLV system, measuring both PR-SRS and PR-2PEF. The results are shown in Fig. 5. In TMA-DPH-MLVs made of DOPC, the order S_2 reported on CH-bonds in labelled MLVs is roughly the same as measured *without* TMA-DPH (Fig. 5a) with $\sigma \approx 80°$. This indicates that at the used concentration $(1:1000)$, the lipid order is not perturbed by the presence of the dyes. A similar effect is seen with the dye di-8-ANEPPS (Fig. 5c). At very high concentration $(10:1000)$ however, a visible increase of the width of the molecular orientational order distribution towards higher order is visible, which indicates that an increased interaction influences slightly the lipid orientational order.

In TMA-DPH-MLVs made of DPPC, there is a stricking difference of orientational order in labelled and unlabelled MLVs (Fig. 5b), with a trend towards a lower orientational order in labelled MLVs ($\sigma \approx 69°$in labelled MLVs as compared to $\sigma \approx 66°$. in unlabelled MLVs, a difference which is small but statistically significant and above the noise limit in S_2). This

results shows that TMA-DPH most probably affects the organization of the DPPC lipids, by favoring a lower constraint of organization. Note that the changes detected with SRS are also visible in CARS but with a lower magnitude (Supporting Table S1), most probably due to the presence of the non-resonant background which organization tends to make CARS less sensitive to a loss of orientational order.

This perturbation of the local orientational order by the presence of a dye is also observed with di-8-ANEPPS-MLVs made of DPPC at identical concentration (1 : 1000), with a very similar behavior (Fig. 5d). The lipid orientational order in labelled MLVs is lower than in unlabelled MLVs. At higher concentration (5 : 1000), the orientational order is seen to decrease further slightly, signature of an influence of di-8-ANEPPS on its local lipid organization. Note that similarly as for TMA-DPH, the molecular orientational order reported by PR-2PEF for di-8-ANEPPS is not entirely correlated with the molecular orientational order changes undergone by their surrounding lipids (Fig. 5b,d). Orientational order values for di-8-ANEPPS are summarized in Supporting Tables S2 and S3.

The influence exerted by lipid probes on their surrounding environment are majorly studied using molecular dynamics simulations. Early studies performed on DPH, the uncharged dye from which TMA-DPH is derived, show that the influence of this lipid probe on the lipids tends towards an opposite trend as reported here (induced higher orientational order), only taking place at the very close proximity of the fluorescence dipole however, with a vanishing effect at larger distance.[33] TMA-DPH being located closer to the surface of lipid bilayers, it is not surprising that its role on the surrounding lipid order is distinct from DPH. The present study investigates also a rather different mesoscopic scale, since hundreds of nanometers laterally are averaged in the measurement. This scale is distinct from previous investigations that explored macroscopic phase transition temperature modifications in the presence of the probe,[34] which illustrates the complexity of quantifying lipid-probe interactions. With the possibility to quantify lipids-related molecular order at intermediate scales between MD and

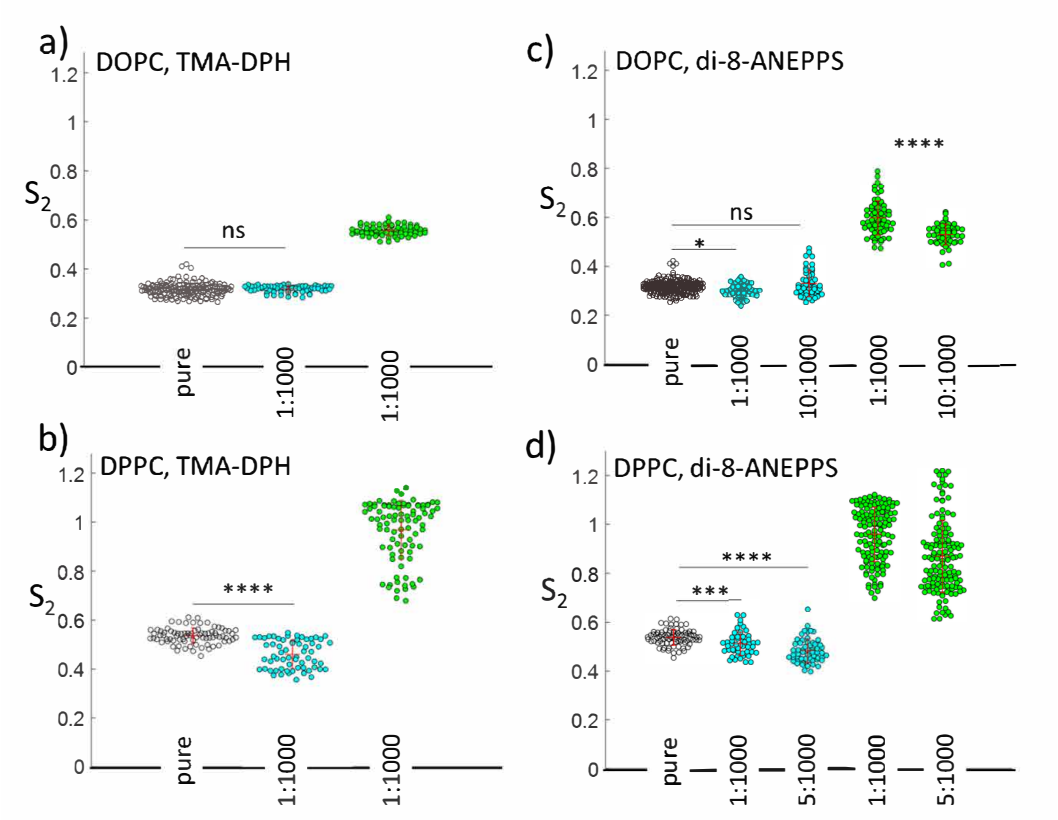

Figure 5: Comparative PR-2PEF and PR-SRS results in unlabelled and labelled MLVs. Beeswarm plots represent S_2 values over all measured pixels in all MLVs, with one marker representing an average over about 100 pixels. (a) TMA-DPH-labelled and unlabelled DOPC lipids. (b) TMA-DPH-labelled and unlabelled DPPC lipids. (c) di-8-ANEPPS-labelled and unlabelled DOPC lipids. (d) di-8-ANEPPS-labelled and unlabelled DPPC lipids. Heterogeneities are seen to occur majorily within MLVs, not in-between MLVs. Number of regions measured (typically 1000 pixels per region): DOPC pure ($N = 16$), DPPC pure ($N = 24$), DOPC labelled ($N = 10$ TMA-DPH, $N = 12$ di-8-ANEPPS $1:1000$, $N = 10$ di-8-ANEPPS $10:1000$), DPPC labelled ($N = 12$ TMA-DPH, $N = 10$ di-8-ANEPPS $1:1000$, $N = 10$ di-8-ANEPPS $5:1000$). Statistical significance was determined using ANOVA tests performed over those populations with ns considered as non-significant, *: $p < 0.05$, **: $p < 0.01$, ***: $p < 0.001$, ****: $p < 0.0001$.

thermodynamics, the methodology proposed in this work is a valuable complementary information on lipids-fluorophores interactions in membranes. The present study shows also that both TMA-DPH and di-8-ANEPPS labelled DPPC MLVs undergo a quite similar trend with a loss of orientational order of the surrounding lipids induced by the presence of the dye. The differences observed in both liquid order (DPPC) and disorder (DOPC) environments for di-8-ANEPPS are relatively in line with previous MD simulations on a close lipid probe, which showed distinct behaviors in ordered and disordered lipid phases.[31] Nevertheless, the present work emphasizes variations with respect to the lipid probe concentration that show a complex influence of lipid probes on their local environment, which require direct experimental access.

In conclusion, we have demonstrated a methodology to bring new insights into the possible influence of fluorescent lipid probes on the lipid environment they are supposed to report on. Being able to probe the extent of such interaction is challenging since detecting lipid probes independently from lipids is not easily accessible in optical microscopy. The combination of label-free and fluorescence polarization resolved approaches proposed in this work quantifies molecular order of CH-bond as a readout of lipids organization modifications, possibly opening to new understanding of lipid/lipid-probes mutual influences.

Acknowledgement

The authors thank Julien Duboisset and Hilton Barbosa de Aguiar for fruitful discussions, as well as Dmitry Nuzhdin for help in the experimental implementation. This work was supported by Centre National de la Recherche Scientifique (CNRS), contracts ANR-15-CE19-0018-01 (MyDeepCARS), ANR-10-INBS-04-01 (France-BioImaging) and Conseil Regional Provence Alpes Cote d'Azur.

Supporting Information Available

Supporting Information contains theoretical and modelling developments for the data analysis of the polarization resolved contrasts in two-photon fluorescence, coherent anti-Stokes Raman scattering and stimulated Raman scattering, as well as Tables of numerical results.

References

(1) Warschawski, D.; Devaux, P. Order parameters of unsaturated phospholipids in membranes and the effect of cholesterol: a 1 H - 13 C solid-state NMR study at natural abundance. *Eur. Biophys. J.* **2005**, *34*, 987–996.

(2) Vermeer, L.; de Groot, B.; Réat, V.; Milon, A.; Czaplicki, J. Acyl chain order parameter profiles in phospholipid bilayers: computation from molecular dynamics simulations and comparison with 2H NMR experiments. *Eur. Biophys. J.* **2007**, *36*, 919–931.

(3) Nagle, J. F.; Tristram-Nagle, S. Structure of lipid bilayers. *Biochim. Biophys. Acta, Rev. Biomembr.* **2000**, *1469*, 159 – 195.

(4) Mashaghi, A.; Mashaghi, S.; Reviakine, I.; Heeren, R. M. A.; Sandoghdar, V.; Bonn, M. Label-free characterization of biomembranes: from structure to dynamics. *Chem. Soc. Rev.* **2014**, *43*, 887–900.

(5) Livanec, P. W.; Dunn, R. C. Single-molecule probes of lipid membrane structure. *Langmuir* **2008**, *24*, 14066–73.

(6) Sezgin, E.; Schwille, P. Fluorescence Techniques to Study Lipid Dynamics. *Cold Spring Harb. Perspect. Biol.* **2011**, *3*.

(7) Winkler, P. M.; Regmi, R.; Flauraud, V.; Brugger, J.; Rigneault, H.; Wenger, J.; García-Parajo, M. F. Optical Antenna-Based Fluorescence Correlation Spectroscopy to Probe

the Nanoscale Dynamics of Biological Membranes. *J. Phys. Chem. Lett.* **2018**, *9*, 110–119.

(8) Lu, J.; Mazidi, H.; Ding, T.; Zhang, O.; Lew, M. D. Single-Molecule 3D Orientation Imaging Reveals Nanoscale Compositional Heterogeneity in Lipid Membranes. *Angew. Chem., Int. Ed.* **2020**, *59*, 17572–17579.

(9) Parasassi, T.; Giusti, A.; Raimondi, M.; Gratton, E. Abrupt modifications of phospholipid bilayer properties at critical cholesterol concentrations. *Biophys. J.* **1995**, *68*, 1895 – 1902.

(10) Klymchenko, A. S.; Kreder, R. Fluorescent Probes for Lipid Rafts: From Model Membranes to Living Cells. *Chem. Biol.* **2014**, *21*, 97–113.

(11) Owen, D. M.; Oddos, S.; Kumar, S.; Davis, D. M.; Neil, M.; French, P. M. W.; Dustin, M. L.; Magee, A. I.; Cebecauer, M. High plasma membrane lipid order imaged at the immunological synapse periphery in live T cells. *Mol. Membr. Biol.* **2010**, *27*, 178–189.

(12) Kenworthy, A. In *Lipid Rafts*; McIntosh, T., Ed.; Methods in Molecular Biology; Humana Press, 2007; Vol. 398; pp 179–192.

(13) Machan, R.; Hof, M. Lipid diffusion in planar membranes investigated by fluorescence correlation spectroscopy. *Biochim. Biophys. Acta, Biomembr.* **2010**, *1798*, 1377 – 1391.

(14) Loura, L.; Fedorov, A.; Prieto, M. Resonance energy transfer in a model system of membranes: application to gel and liquid crystalline phases. *Biophys. J.* **1996**, *71*, 1823 – 1836.

(15) Axelrod, D. Carbocyanine dye orientation in red cell membrane studied by microscopic fluorescence polarization. *Biophys. J.* **1979**, *26*, 557–73.

(16) Brasselet, S. Polarization-resolved nonlinear microscopy: application to structural molecular and biological imaging. *Adv. Opt. Photon.* **2011**, *3*, 205–271.

(17) Benninger, R.; Önfelt, B.; Neil, A. A. M.; Davis, M. D.; French, P. M. W. Fluorescence Imaging of Two-Photon Linear Dichroism: Cholesterol Depletion Disrupts Molecular Orientation in Cell Membranes. *Biophys. J.* **2005**, *88*, 609–622.

(18) Brasselet, S.; Ferrand, P.; Kress, A.; Wang, X.; Ranchon, H.; Gasecka, A. In *Fluorescent Methods to Study Biological Membranes*; Mély, Y., Duportail, G., Eds.; Springer Berlin Heidelberg: Berlin, Heidelberg, 2013; pp 311–337.

(19) Ferrand, P.; Gasecka, P.; Kress, A.; Wang, X.; Bioud, F.-Z.; Duboisset, J.; Brasselet, S. Ultimate Use of Two-Photon Fluorescence Microscopy to Map Orientational Behavior of Fluorophores. *Biophys. J.* **2014**, *106*, 2330 – 2339.

(20) Gasecka, A.; Han, T.-J.; Favard, C.; Cho, B. R.; Brasselet, S. Quantitative Imaging of Molecular Order in Lipid Membranes Using Two-Photon Fluorescence Polarimetry. *Biophys. J.* **2009**, *97*, 2854 – 2862.

(21) Reeve, J. E.; Corbett, A. D.; Boczarow, I.; Wilson, T.; Bayley, H.; Anderson, H. L. Probing the orientational distribution of dyes in membranes through multiphoton microscopy. *Biophy.s J.* **2012**, *103*, 907–917.

(22) Benninger, R.; Vanherberghen, B.; Young, S.; Taner, S. B.; Culley, F. J.; Schnyder, T.; Neil, A. A. M.; Wüstner, D.; French, P. M. W.; Davis, D. M. et al. Live cell linear dichroism imaging reveals extensive membrane ruffling within the docking structure of natural killer cell immune synapses. *Biophys. J.* **2009**, *96*, L13–5.

(23) Kress, A.; Wang, X.; Ranchon, H.; Savatier, J.; Rigneault, H.; Ferrand, P.; Brasselet, S. Mapping the Local Organization of Cell Membranes Using Excitation-Polarization-Resolved Confocal Fluorescence Microscopy. *Biophys. J.* **2013**, *105*, 127 – 136.

(24) Ben-Yashar, V.; Menashe, M.; Biltonen, R. L.; Johnson, M. L.; Barenholz, Y. Interaction of trans-parinaric acid with phosphatidylcholine bilayers: comparison with the effect of other fluorophores. *Biochim. Biophys. Acta* **1987**, *904*, 117–24.

(25) Lentz, B. R. Use of fluorescent probes to monitor molecular order and motions within liposome bilayers. *Chem. Phys. Lipids* **1993**, *64*, 99–116.

(26) Leonard-Latour, M.; Morelis, R. M.; Coulet, P. R. Influence of Pyrene-Based Fluorescent Probes on the Characteristics of DMPA/DMPC LangmuirBlodgett Films. *Langmuir* **2004**, *12*, 4797–4802.

(27) Bouvrais, H.; Pott, T.; Bagatolli, L. A.; Ipsen, J. H.; Méléard, P. Impact of membrane-anchored fluorescent probes on the mechanical properties of lipid bilayers. *Biochim. Biophys. Acta, Biomembr.* **2010**, *1798*, 1333–1337, Microscopy Imaging of Membrane Domains.

(28) Koivusalo, M.; Alvesalo, J.; Virtanen, J. A.; Somerharju, P. Partitioning of Pyrene-Labeled Phospho- and Sphingolipids between Ordered and Disordered Bilayer Domains. *Biochim. Biophys. Acta* **2004**, *86*, P923–935.

(29) Vogel, A.; Scheidt, H. A.; Huster, D. The distribution of lipid attached spin probes in bilayers: application to membrane protein topology. *Biophys. J.* **2003**, *85*, 1691–701.

(30) Suhaj, A.; Le Marois, A.; Williamson, D. J.; Suhling, K.; Lorenz, C. D.; Owen, D. M. PRODAN differentially influences its local environment. *Phys. Chem. Chem. Phys.* **2018**, *20*, 16060–16066.

(31) Suhaj, A.; Gowland, D.; Bonini, N.; Owen, D. M.; Lorenz, C. D. Laurdan and Di-4-ANEPPDHQ Influence the Properties of Lipid Membranes: A Classical Molecular Dynamics and Fluorescence Study. *J. Phys. Chem. B* **2020**, *124*, 11419–11430.

(32) Filipe, H. A. L.; Moreno, M. J.; Loura, L. M. S. The Secret Lives of Fluorescent Membrane Probes as Revealed by Molecular Dynamics Simulations. *Molecules* **2020**, *25*.

(33) Repáková, J.; Holopainen, J. M.; Morrow, M. R.; McDonald, M. C.; Čapková, P.; Vattulainen, I. Influence of DPH on the Structure and Dynamics of a DPPC Bilayer. *Biophys. J.* **2005**, *88*, 3398–3410.

(34) Ambrosini, A.; Tanfani, F.; Bertoli, E.; Wozniak, M.; Wypych, Z.; Zolese, G. Effect of N-acylethanolamines with different acyl-chains on DPPC multilamellar liposomes. *Chem. Phys. Lipids* **1993**, *65*, 165–169.

(35) Zumbusch, A.; Holtom, G. R.; Xie, X. S. Three-Dimensional Vibrational Imaging by Coherent Anti-Stokes Raman Scattering. *Phys. Rev. Lett.* **1999**, *82*, 4142–4145.

(36) Evans, C.; Xie, X. Coherent Anti-Stokes Raman Scattering Microscopy: Chemical Imaging for Biology and Medicine. *Annu. Rev. Anal. Chem.* **2008**,

(37) Freudiger, C. W.; Min, W.; Saar, B. G.; Lu, S.; Holtom, G. R.; He, C.; Tsai, J. C.; Kang, J. X.; Xie, X. S. Label-Free Biomedical Imaging with High Sensitivity by Stimulated Raman Scattering Microscopy. *Science* **2008**, *322*, 1857–1861.

(38) Nandakumar, P.; Kovalev, A.; Volkmer, A. Vibrational imaging based on stimulated Raman scattering microscopy. *New J. Phys.* **2009**,

(39) Potma, E. O.; Xie, X. S. Detection of single lipid bilayers with coherent anti-Stokes Raman scattering (CARS) microscopy. *J. Raman Spectrosc.* **2003**, *34*, 642–650.

(40) Wurpel, G. W. H.; Schins, J. M.; Müller, M. Direct Measurement of Chain Order in Single Phospholipid Mono- and Bilayers with Multiplex CARS. *J. Phys. Chem. B* **2004**, *108*, 3400–3403.

(41) Potma, E. O.; Xie, X. S. Direct Visualization of Lipid Phase Segregation in Single Lipid Bilayers with Coherent Anti-Stokes Raman Scattering Microscopy. *ChemPhysChem* **2005**, *6*, 77–79.

(42) Müller, M.; Schins, J. M. Imaging the Thermodynamic State of Lipid Membranes with Multiplex CARS Microscopy. *J. Phys. Chem. B* **2002**, *106*, 3715–3723.

(43) Wurpel, G.; Rinia, H.; Müller, M. Imaging orientational order and lipid density in multilamellar vesicles with multiplex CARS microscopy. *J. Microsc.* **2005**, *218*, 37–45.

(44) Bioud, F.-Z.; Gasecka, P.; Ferrand, P.; Rigneault, H.; Duboisset, J.; Brasselet, S. Structure of molecular packing probed by polarization-resolved nonlinear four-wave mixing and coherent anti-Stokes Raman-scattering microscopy. *Phys. Rev. A* **2014**, *89*, 013836.

(45) Duboisset, J.; Berto, P.; Gasecka, P.; Bioud, F.-Z.; Ferrand, P.; Rigneault, H.; Brasselet, S. Molecular Orientational Order Probed by Coherent Anti-Stokes Raman Scattering (CARS) and Stimulated Raman Scattering (SRS) Microscopy: A Spectral Comparative Study. *J. Phys. Chem. B* **2015**, *119*, 3242–3249.

(46) Fu, Y.; Huff, T. B.; Wang, H.-W.; Cheng, J.-X.; Wang, H. Ex vivo and in vivo imaging of myelin fibers in mouse brain by coherent anti-Stokes Raman scattering microscopy. *Opt. Express* **2008**, *16*, 19396–19409.

(47) de Vito, G.; Bifone, A.; Piazza, V. Rotating-polarization CARS microscopy: combining chemical and molecular orientation sensitivity. *Opt. Express* **2012**, *20*, 29369–29377.

(48) Turcotte, R.; Rutledge, D. J.; Bélanger, E.; Dill, D.; Macklin, W. B.; Côté, D. C. Intravital assessment of myelin molecular order with polarimetric multiphoton microscopy. *Sci. Rep.* **2016**, *6*, 31685.

(49) Gasecka, P.; Jaouen, A.; Bioud, F.-Z.; Barbosa de Aguiar, H.; Duboisset, J.; Ferrand, P.; Rigneault, H.; Balla, N. K.; Debarbieux, F.; Brasselet, S. Lipid Order Degradation in

Autoimmune Demyelination Probed by Polarized Coherent Raman Microscopy. *Biophys. J.* **2017**, *113*, 1520–1530.

(50) de Vito, G.; Cappello, V.; Tonazzini, I.; Cecchini, M.; Piazza, V. RP-CARS reveals molecular spatial order anomalies in myelin of an animal model of Krabbe disease. *J. Biophoton.* **2017**, *10*, 385–393.

(51) Wang, Z.; Zheng, W.; Hsu, C.-Y. S.; Huang, Z. Polarization-resolved hyperspectral stimulated Raman scattering microscopy for label-free biomolecular imaging of the tooth. *Appl. Phys. Lett.* **2016**, *108*, 033701.

(52) Kerdoncuff, H.; Pollard, M. R.; Westergaard, P. G.; Petersen, J. C.; Lassen, M. Compact and versatile laser system for polarization-sensitive stimulated Raman spectroscopy. *Opt. Express* **2017**, *25*, 5618–5625.

(53) Hofer, M.; Balla, N. K.; Brasselet, S. High-speed polarization-resolved coherent Raman scattering imaging. *Optica* **2017**, *4*, 795–801.

(54) Nahmad-Rohen, A.; Regan, D.; Masia, F.; McPhee, C.; Pope, I.; Langbein, W.; Borri, P. Quantitative Label-Free Imaging of Lipid Domains in Single Bilayers by Hyperspectral Coherent Raman Scattering. *Anal. Chem.* **2020**, *92*, 14657–14666.

(55) Loew, L. M.; Cohen, L. B.; Dix, J.; Fluhler, E. N.; Montana, V.; Salama, G.; Wu, J. Y. A naphthyl analog of the aminostyryl pyridinium class of potentiometric membrane dyes shows consistent sensitivity in a variety of tissue, cell, and model membrane preparations. *J. Membr. Biol.* **1992**, *130*, 1–10.

(56) Lentz, B. R. Membrane "fluidity" as detected by diphenylhexatriene probes. *Chem. Phys. Lipids* **1989**, *50*, 171–190.

(57) Haluska, C. K.; Schröder, A. P.; Didier, P.; Heissler, D.; Duportail, G.; Mély, Y.; Marques, C. M. Combining Fluorescence Lifetime and Polarization Microscopy to Dis-

criminate Phase Separated Domains in Giant Unilamellar Vesicles. *Biophys. J.* **2008**, *95*, 5737 – 5747.

(58) do Canto, A. M.; Robalo, J. R.; Santos, P. D.; Carvalho, A. J. P.; Ramalho, J. P.; Loura, L. M. Diphenylhexatriene membrane probes DPH and TMA-DPH: A comparative molecular dynamics simulation study. *Biochim. Biophys. Acta. Biomembr.* **2016**, *1858*, 2647–2661.

(59) Bangham, A.; Hill, M.; Miller, N. In *Methods in Membrane Biology*; Korn, E., Ed.; Springer US, 1974; pp 1–68.

(60) Ferrand, P. GPScan.VI: A general-purpose LabVIEW program for scanning imaging or any application requiring synchronous analog voltage generation and data acquisition. *Comput. Phys. Commun.* **2015**, *192*, 342 – 347.

(61) de Aguiar, H. B.; Gasecka, P.; Brasselet, S. Quantitative analysis of light scattering in polarization-resolved nonlinear microscopy. *Opt. Express* **2015**, *23*, 8960–8973.

(62) Mansfield, J. C.; Littlejohn, G. R.; Seymour, M. P.; Lind, R. J.; Perfect, S.; Moger, J. Label-free Chemically Specific Imaging in Planta with Stimulated Raman Scattering Microscopy. *Anal. Chem.* **2013**, *85*, 5055–5063.

(63) Cheng, J. X.; Pautot, S.; Weitz, D. A.; Xie, X. S. Ordering of water molecules between phospholipid bilayers visualized by coherent anti-Stokes Raman scattering microscopy. *Proc. Natl. Acad. Sci. U.S.A.* **2003**, *100*, 9826–9830.